Localized Corrosion of Mild Steel in Marginally Sour Environments

Saba Navabzadeh Esmaeely,[‡,]* Wei Zhang,* Bruce Brown,* Marc Singer,* and Srdjan Nešić*

ABSTRACT

Localized corrosion has been a challenge for the integrity of mild steel pipelines, specifically at operating conditions where a trace amount of H$_2$S is present alongside CO$_2$ at lower temperatures. The presence of H$_2$S will lead to the formation of a protective iron sulfide layer that will decrease the general corrosion rate; however, a trace amount of H$_2$S may only form a partially protective mackinawite layer that could result in localized corrosion. In the current study, mild steel specimens (API 5L X65) were exposed to a 1 wt% NaCl solution sparged at 0.096 MPa pCO$_2$ and 15×10^{-6} MPa or less pH$_2$S (≤150 ppm H$_2$S/CO$_2$). At pH 5.0 and 30°C the bulk solution was undersaturated with respect to iron sulfide—mackinawite and iron carbonate. At these marginally sour conditions, a H$_2$S/CO$_2$ threshold of approximately 100 ppm was deduced, below which localized corrosion happened. No localized corrosion occurred for the same environmental conditions when H$_2$S/CO$_2$ ratio was above 100 ppm or when there was no H$_2$S present.

KEY WORDS: *carbides, carbon dioxide, hydrogen sulfide, localized corrosion, marginally sour*

INTRODUCTION

Localized corrosion presents a threat to the integrity of mild steel pipelines and equipment in the oil and gas industry, given that it often proceeds at a much faster rate than uniform corrosion at the same conditions. It frequently results in failure, when the penetration depth exceeds far beyond the built-in corrosion allowance, which is based on the predicted uniform corrosion rates. The lack of ability to predict localized corrosion and to detect it by using conventional corrosion monitoring methods makes a difficult situation even worse.

Because the presence of H$_2$S in upstream oil and gas pipelines has been associated with an increased risk of localized corrosion,[1] a significant research effort has been focused on understanding H$_2$S corrosion mechanisms. Mild steel corrosion in such environments has been investigated since the 1940s, and was mostly concentrated on uniform corrosion.[2-19] Rather few studies available in the open literature have addressed localized corrosion in H$_2$S-containing environments. There, most of the effort was on aqueous solutions that contain moderate to high amounts of H$_2$S (pH$_2$S = 0.01 MPa to 0.5 MPa) with temperatures ranging from 50°C to 150°C.[20-24]

There are two postulated mechanisms of localized corrosion in H$_2$S environments: the first one associated with the presence of elemental sulfur[25-28] and the second one related to formation of conductive iron sulfides, such as pyrite and pyrrhotite, in the corrosion product layer.[29-34] Both of these mechanisms result in galvanic corrosion and are typical for conditions with higher H$_2$S partial pressures and higher temperatures, such as those listed above. The presence of chloride was also listed as a risk factor for localized corrosion in H$_2$S-containing environments.[35] One explanation is that chloride impact is via changing the electrolyte conductivity and iron sulfide solubility, which are directly linked to the two abovementioned mechanisms.[36]

In the oil and gas industry, one frequently encounters conditions with lower temperatures and only trace amounts of H_2S (in the ppm range), which are also referred to as "marginally sour" conditions. One example is sweet wells which become marginally sour over the lifetime of production, resulting from microbiological (sulfate-reducing bacteria) activity in the reservoir.[37] Under these marginally sour conditions, CO_2 is the main cause of corrosion and it has been suggested that trace amounts of H_2S lead to formation of a thin iron sulfide corrosion product layer, which has protective properties.[22,38] Therefore, uniform corrosion rates of mild steel in marginally sour conditions were found to be lower than those seen under the same conditions without H_2S. An early example was given by Lee,[38] where with only 3 ppm H_2S/CO_2 (at atmospheric pressure) the sweet corrosion rate was halved, while at 15 ppm and higher the corrosion rate was almost an order of magnitude lower compared to conditions where there was no H_2S.

Despite this apparently beneficial effect of a trace amount of H_2S on uniform corrosion of mild steel, there are some indications that such conditions might lead to a serious risk of localized attack. In a recent study, focused on top-of-the-line corrosion in sour environments, Yaakob, et al.,[39-40] reported localized corrosion at 15 ppm and 30 ppm H_2S, at room temperature and 1 MPa CO_2 partial pressure. In the same study localized corrosion was not observed at 80 ppm and 150 ppm H_2S. This seems to suggest that there may be a threshold concentration of H_2S below which localized corrosion occurs in marginally sour environments.

It is therefore of importance to investigate whether such a threshold exists. In an effort to prove this, the experiments described below were conducted with trace amounts of H_2S at low temperature (30°C). The experiments were conducted in a small scale glass cell at atmospheric pressure.

EXPERIMENTAL METHOD

Experiments were conducted in a conventional three-electrode glass cell[41] with the experimental conditions summarized in Table 1. In this setup, the cylindrical cell was filled with 2 L of deionized (DI) water and 20.2 g of sodium chloride (NaCl) to obtain a 1.0 wt% NaCl electrolyte. The temperature was set to room temperature (30°C). Electrochemical measurements were conducted using a three-electrode setup with a 5.4 cm^2 API 5 L X65 (tempered martensitic microstructure), with elemental analysis given in Table 2, serving as the working electrode (WE). A platinum mesh plate was used as the counter electrode (CE). A saturated silver/silver chloride (Ag/AgCl) reference electrode (RE) was connected via a Luggin capillary. The H_2S gas concentration at the inlet was adjusted using gas rotameters and the accuracy was confirmed by taking a gas sample using a pump with colorimetric

† Trade name.

TABLE 1
Experimental Matrix - Glass Cell

Parameters	Conditions
Total pressure	0.1 MPa
Temperature	30°C
Solution	1 wt% NaCl
Flow condition	Agitated, 300 rpm 0.5 in (1.27 cm) stir bar
Material	API 5L X65 steel
Corrosion measurement methods	LPR, EIS, and weight loss
pCO$_2$	0.096 MPa
pH$_2$S in the gas phase	0
	4×10^{-6} MPa (40 ppm)
	9×10^{-6} MPa (90 ppm)
	15×10^{-6} MPa (150 ppm)
pH	5.0±0.1

TABLE 2
API 5L X65 Elemental Analysis (wt%)

C	Mn	Si	P	S	Cr	V	Ni	Mo	Al	Fe
0.13	1.16	0.26	0.009	0.009	0.14	0.047	0.36	0.16	0.032	Balance

H_2S detector tubes. The gas outlet was scrubbed through a 1 M sodium hydroxide solution (NaOH) and a dry carbon scrubber to capture H_2S.

In order to ensure that the solution was deoxygenated, it was purged with CO_2 gas for at least 2 h prior to adding H_2S gas at the desired concentration. The solution pH was set to pH 5.0 by adding a deoxygenated 1 M sodium hydroxide (NaOH) solution. The electrolyte was stirred at 300 rpm with a 0.5 in (1.27 cm) stir bar to ensure mixing.

In addition to the cylindrical WE, flat square specimens, with a surface area of 3.4 cm^2 and made from the same material, were suspended in the solution for the purpose of measuring weight loss and performing surface analysis. Prior to immersion all specimens were sequentially polished with silicon carbide sandpaper from 150 grit to 600 grit, rinsed with DI water, cleaned with isopropanol in an ultrasonic bath, and air dried and weighed.

The corrosion process was monitored by recording the open-circuit potential (OCP), and by performing linear polarization resistance (LPR) and electrochemical impedance spectroscopy (EIS) measurements using a Gamry Reference 600† potentiostat. The polarization resistance (Rp) was obtained by polarizing the WE, sweeping the potential from 5 mV below the OCP to 5 mV above the OCP at a scan rate of 0.125 mV/s. The B value of 23 mV was used in all cases to calculate the LPR corrosion rate. The Rp was corrected for ohmic drop using the solution resistance (Rs) measured by EIS at high frequencies (ca. 5 kHz).

Surface and compositional analyses were performed using scanning electron microscopy (SEM) and x-ray diffraction (XRD), respectively. XRD analyses were executed through a CuKα source (λ = 1.5405 Å = 0.154 nm, 40 kV and 44 mA), scanning from 10 2θ

to 70 2θ at a scan rate of 1° per min. An Alicona Infini-teFocus[†] profilometer microscope was utilized to measure the pit depth after the corrosion product layer was chemically removed. The Fe^{2+} concentrations were measured by ultraviolet-visible (UV-vis) spectrophotometry.

RESULTS

For each of the H_2S concentrations, the experiments were repeated at least three times except for the experiment with 150 ppm H_2S that was conducted twice. The uniform corrosion rates and the measured OCP are shown in Figure 1 as a function of time. The points are averages across the different repeats. The error bars denote the maximum and the minimum deviation from the average value.

The measured OCP (Figure 1[a]) of each specimen shows a potential increase between 30 mV and 50 mV. This could be as a result of two possible mechanisms, an increase in the cathodic reaction rate or a decrease in the anodic reaction rate.

In the absence of H_2S, the CO_2 LPR corrosion rate increased over time (Figure 1[b]). This was a result of the iron carbide, the part of the steel structure that is left on the steel surface as it does not corrode. It is well known that iron carbide is conductive and therefore this porous layer increases the cathodic surface area, and as a result of a galvanic effect it leads to an increase in the corrosion current/rate.[42-45] This was reflected in the measured Rp, however, the magnitude of the corrosion rate increase is overestimated there, as the LPR method cannot properly account for different cathodic and anodic surface areas. The increase in the cathodic reaction rate also explains the positive shift in the specimen OCP shown in Figure 1(a).

For the two conditions at 40 ppm and 90 ppm H_2S, the LPR corrosion rate (Figure 1[b]) started out lower than in the absence of H_2S, resulting from formation of a protective iron sulfide—mackinawite layer. The corrosion rate decreased further during the first day of exposure and then increased until the end of the experiment. One would be tempted to ascribe this increase to iron carbide layer formation, however, most of the surface was covered by a significantly thin layer, possibly made of a mixture of mackinawite and iron carbide, which could not produce any significant galvanic current. Another possibility is non-uniform attack that initiated and developed over time. As LPR records the total current that is averaged across the surface area of the specimen, any failure of the protective mackinawite layer and localized attack would present itself as an apparent increase in the LPR corrosion rate. Without proper surface analysis this assumption cannot be confirmed.

For the experiment conducted with 150 ppm H_2S, the LPR corrosion rate decreased upon exposure and stayed low over the course of the experiment. This could be an indication of a more protective mackinawite
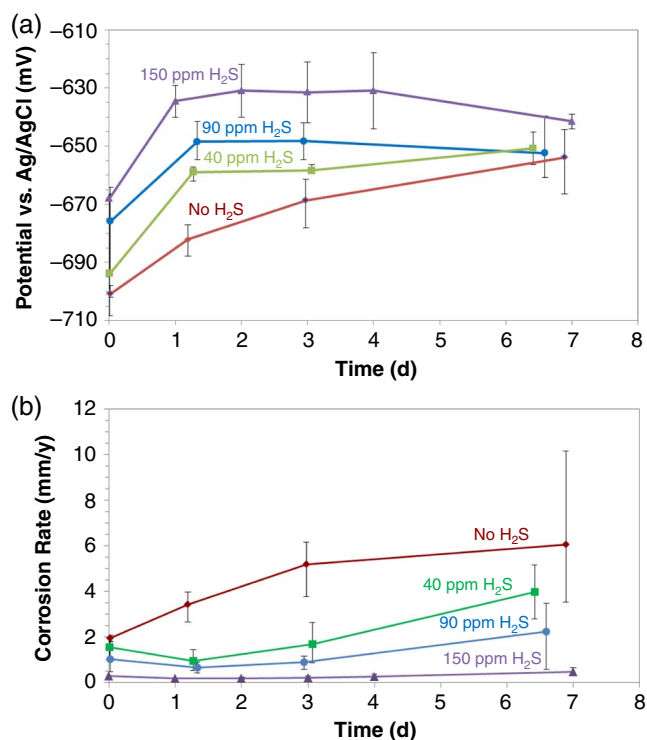

FIGURE 1. (a) Open-circuit potential, (b) linear polarization resistance corrosion rate from X65 specimen in a 1 wt% NaCl, CO_2 saturated solution at 30°C, pH5 at 0.1 MPa total pressure, with and without H_2S.

layer which formed at this higher H_2S concentration. The lower LPR corrosion rates seen in the presence of H_2S are the result of a retardation of the anodic reaction that resulted in a positive shift on the OCP seen in Figure 1(a).

Figure 2 shows the changes in bulk solution properties over the course of the experiments. Figure 2(a) shows the pH variation; in order to keep the bulk pH value relatively stable, diluted deoxygenated HCl was occasionally injected into the experimental cell. Figures 2(b) and (c) show calculated saturation values with respect to iron carbonate[46] (Equation [1]) and mackinawite[47] (Equation [2]), respectively.

$$S_{FeCO_3} = \frac{C_{Fe^{2+}} C_{CO_3^{2-}}}{C_{H^+} K_{sp,FeCO_3}} \tag{1}$$

$$K_{sp,FeCO_3} = -59.3498 - 0.041377\,T - \frac{2.1963}{T}$$
$$+ 24.5724\log(T) + 2.518\,I^{0.5} - 0.657\,I \tag{2}$$

$$S_{FeS(Mackinawite)} = \frac{C_{Fe^{2+}} C_{HS^-}}{C_{H^+} K_{sp,FeS(Mackinawite)}} \tag{3}$$

$$K_{sp,FeS(mackinawite)} = 10^{\frac{2848.779}{T} - 6.347 + \log(K_1)} \tag{4}$$

$$K_{(H_2S)}$$
$$= 10^{\left(782.43945 + 0.361261\,T_K - 1.6722 \cdot 10^{-4} T_K^2 \frac{20565.7315}{T_K} - 142.741722\ln T_K\right)} \tag{5}$$
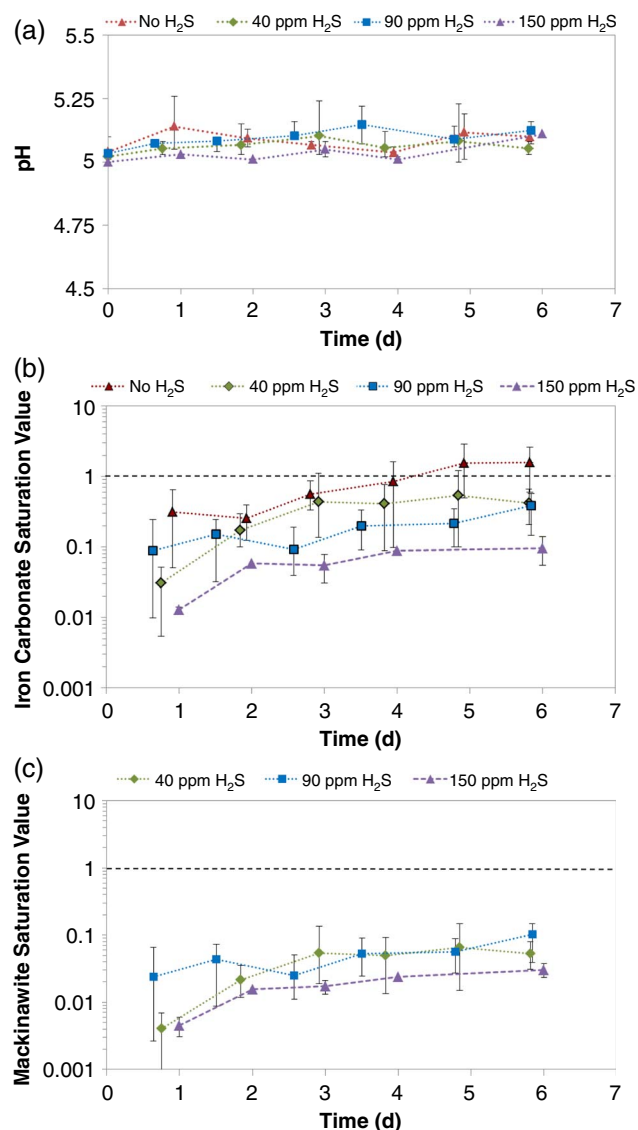
FIGURE 2. *(a) pH variation, (b) iron carbonate saturation degree, and (c) mackinawite saturation degree of the bulk solution during the experiments; 1 wt% NaCl CO_2 saturated solution at 30°C with at 0.1 MPa total pressure, with and without H_2S.*

where $C_{FE^{2+}}$, $C_{CO_3^{2-}}$, C_{HS^-}, and C_{H^+} are the ion concentrations for ferrous iron, carbonate, bisulfide, and hydrogen ions in mol/L, respectively. K_{sp} stands for the solubility limit, T is temperature (K), I is the ionic strength, and K_1[48] is the first dissociation constant of H_2S (mol/L). In all of the experiments, the bulk solution was undersaturated with respect to both iron carbonate and mackinawite. It should be emphasized that the surface pH is expected to be higher than the bulk pH which would result in higher saturation values in the vicinity of the corroding surface. It has been previously shown that the surface pH could vary from the bulk pH by 1 unit to 2 units depending on the level of mixing.[49] This suggests that both iron carbonate and mackinawite were likely supersaturated at the steel surface,

which is a necessary precondition for formation of solid corrosion products layers.

Figure 3 shows the SEM images of the surface of exposed specimens. In the absence of H_2S, a fractured layer on the surface is observed (Figure 3[a]). With H_2S present, the specimen surface was covered with a thin compact layer that seems to be following the original shape of the steel surface including the polishing marks. For the case of 40 ppm and 90 ppm H_2S there are some local failures of the layer, which can be seen in Figures 3(b) and (c). The surface of the specimen exposed to 150 ppm H_2S does not show any such features (Figure 3[d]).

XRD was utilized in order to identify the makeup of the corrosion product layer. Iron carbide was identified on the specimen exposed to a solution without H_2S (Figure 4[a]). However, the XRD patterns of the specimens exposed to 40 ppm and 90 ppm H_2S do not show any peaks that could correspond to mackinawite, iron carbonate, nor iron carbide (Figures 4[b] and [c]). The peaks on these two patterns at 44 2θ and 65 2θ are the α Fe peaks.[50] This shows that the layers formed on these surfaces were so thin (order of μm) that the conventional XRD was not able to detect the layer. XRD was not conducted on the specimen exposed to 150 ppm H_2S. The elemental analysis using EDS showed sulfur on the surface of the specimens exposed to 40 ppm, 90 ppm, and 150 ppm H_2S after 6 d to 7 d of exposure.

Cross-section images of the specimens were analyzed in order to investigate the corrosion product layer thickness and the appearance of the pits. The specimen exposed to the aqueous CO_2 solution (in the absence of H_2S) shown in Figure 5(a) has a very porous and detached fragmented layer on the surface, which is made of iron carbide and lacks any protective properties. The specimens exposed to 40 ppm and 90 ppm H_2S are shown in Figures 5(b) and (c), respectively, showing pitting. These pits are partially filled with some corrosion product, which is not dense, nor is it well attached; therefore, it is likely that these pits had remained active throughout the experiment. A very thin layer is seen on the steel surface in the vicinity of the pits, which explains the inability of the XRD to detect this layer. The specimen exposed to 150 ppm H_2S is shown in Figure 5(d), where a very thin layer is present. No pitting was found on this surface.

In order to investigate the morphology of the corrosion attack, the corrosion product layer was chemically removed following the procedure given in ASTM Standard G1[51] using Clarke's solution. Figure 6 shows the SEM images of the specimen surface after the corrosion product layer was removed. Figure 6(a) shows the specimen exposed to aqueous CO_2 in the absence of H_2S and exhibits a relatively rough surface, which shows that the specimen underwent severe uniform corrosion. The specimens exposed to 40 ppm
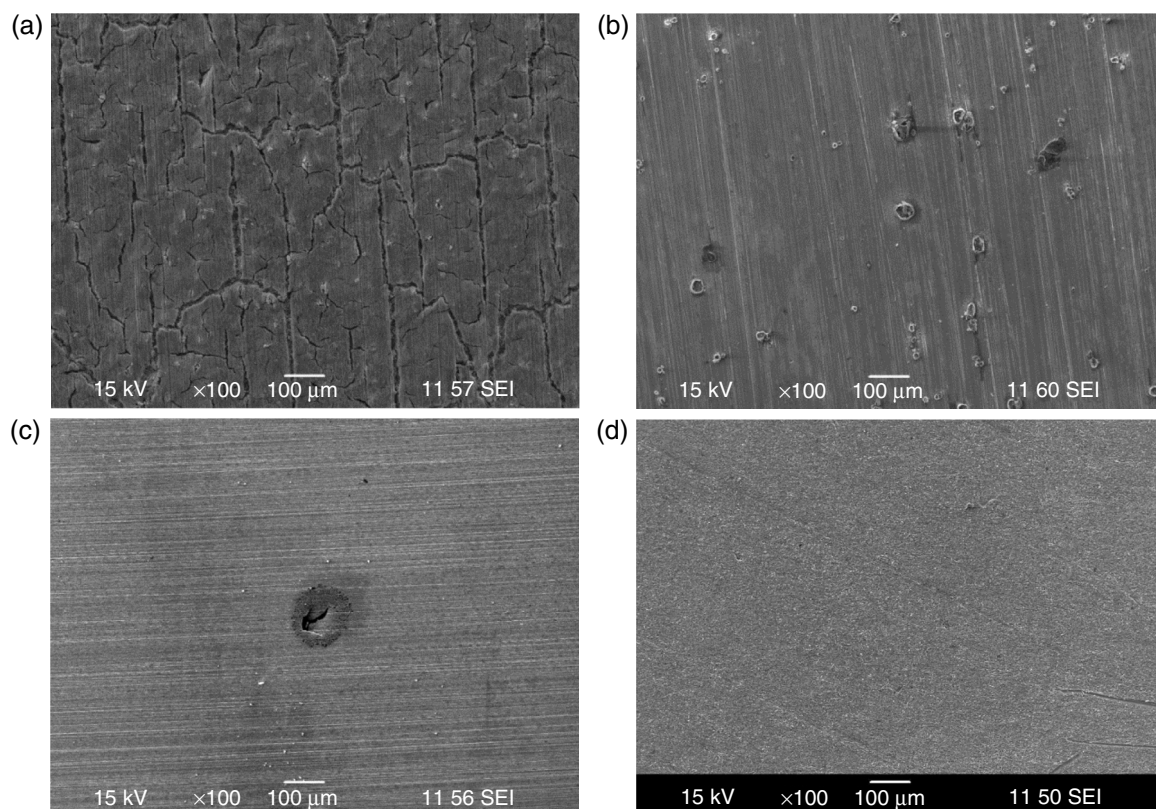
FIGURE 3. *SEM image of recovered X65 specimens after 6 d of exposure to an aqueous solution sparged with (a) no H_2S, (b) 40 ppm H_2S, (c) 90 ppm H_2S, and (d) 150 ppm H_2S in CO_2 at 30°C and pH 5.0, 1 wt% NaCl, 6 d exposure.*

and 90 ppm H_2S still have the original polishing marks on the majority of the surface, along with locally corroded areas (Figures 6[b] and [c]). There are much smaller and shallower pits on the specimen exposed to 150 ppm H_2S in Figure 6(c).

Profilometry was utilized to measure the depth of the pits on the surface and the deepest pit depth was used to calculate the maximum pit penetration rate (PPR) (Figure 7). The specimen exposed to aqueous CO_2 solution (in the absence of H_2S) does not show any features on the surface that could be considered as localized attack, just general roughening. The profilometry of the specimens exposed to 40 ppm and 90 ppm H_2S shows evidence of pitting, more widespread at 40 ppm. A pit depth of more than 200 µm can be seen on both specimens in Figures 7(b) and (c). The image of the specimen exposed to 150 ppm H_2S shows very small pits with the depth less than 10 µm, which cannot be considered as localized corrosion.

The specimens were weighed after the corrosion product layer was removed; the time averaged weight loss corrosion rate ($\Delta m/t$ in mm/y) and the PPR of the specimens versus the H_2S concentration are compared in Figure 8. The data show that the overall mass loss decreased with an increase in H_2S

concentrations; however, 40 ppm and 90 ppm H_2S triggered localized corrosion. For these two experiments, the PPR was at least five times higher than the uniform corrosion rate of the specimen exposed to similar aqueous environment without H_2S confirming localized corrosion.[52] In the presence of 150 ppm H_2S, localized corrosion was not observed and the weight loss corrosion rate shows the lowest value as compared with other experiments.

DISCUSSION

It was shown above that localized corrosion occurred on mild steel specimens exposed to aqueous CO_2 solutions with trace amounts of H_2S. The bulk solution in all experiments was undersaturated with respect to corrosion products: iron carbonate and mackinawite. However, a corrosion product layer was observed on the corroded specimen SEM images. Based on XPS analysis reported by Lee and Nend[53-54] and Choi, et al.,[19] it is likely that the layer was mackinawite. This was not unexpected, because a corrosion process results in different water chemistry at the surface as compared to the bulk, with both the pH and Fe^{2+} concentrations being higher at the corroding steel surface.[49] This is particularly pronounced in
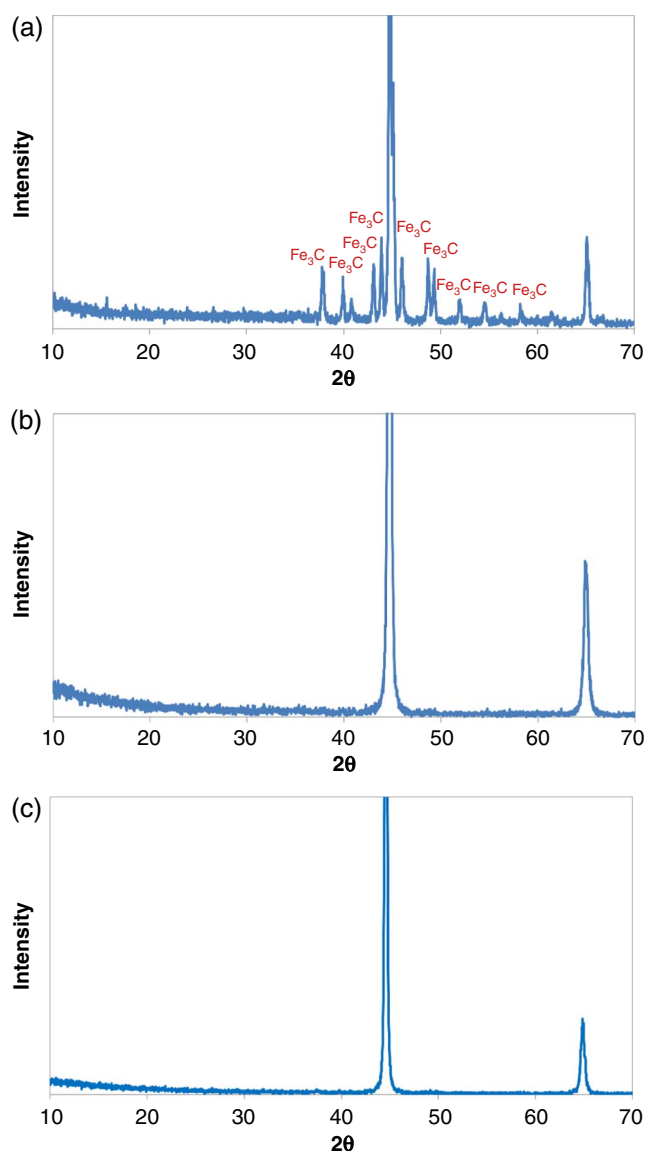
FIGURE 4. *X-ray diffraction of the recovered X65 after 6 d exposure to a saturated CO_2 solution at 30°C and pH 5.0: (a) no H_2S, (b) 40 ppm H_2S, and (c) 90 ppm H_2S, 1 wt% NaCl.*

quiescent conditions, while the surface and the bulk water chemistry values converge in turbulent flow conditions.

In marginally sour environments, such as the one used in the current study, the higher pH and Fe^{2+} concentration at the surface allowed mackinawite layer formation, even if the bulk solution was undersaturated. As the mackinawite layer formed and grew in thickness it presented a diffusion barrier, which led to a reduction in the corrosion rate. Because of ongoing corrosion that was undermining the layer, it did not form uniformly.[55] It is well known that protectiveness of a corrosion product layer depends on the so-called scaling tendency, which is a ratio of the precipitation rate and the corrosion rate.[56] When the scaling tendency is high, the precipitation overwhelms corrosion and protective

layers form. Conversely, when rapid corrosion overpowers the precipitation and undermines the layer, nonprotective layers form. In the current study, when there was more H_2S, the precipitation proceeded at a faster rate, thus a more protective layer formed and vice versa. At lower H_2S concentrations, faults in the layer allowed the corrosive species to reach the steel surface. This resulted in localized corrosion at those locations. In addition, the outer surface of the growing mackinawite underwent dissolution. Therefore, the stability of this layer depended on the balance of: undermining by corrosion, precipitation at the steel/mackinawite interface, and dissolution at the mackinawite/solution interface.

The observed localized corrosion rates in the present study were higher than the bare steel corrosion rate exposed to similar conditions without the presence of H_2S. It should be noted that while H_2S provided partial protection in these marginally sour environments, it would not have significantly contributed to the uniform corrosion rate because of the very low concentrations. It was the much higher content of CO_2 that led to the high corrosion rate (the corrosiveness of carbonic acid has been well documented).[57] However, iron carbonate, which is the product of CO_2 corrosion, was not found at the surface of the steel under these conditions because of a much slower kinetics of formation when compared to that of mackinawite.[58] Therefore, it is believed that the observed localized corrosion was the result of a galvanic effect. The galvanic effect was driven by a positive shift in the surface potential[59] at the mackinawite-covered steel surface (Figure 1[a]). It is not entirely clear at this time whether the increase in potential was the result of an increase of the cathodic surface area, or due to the retardation of the anodic reaction as a result of coverage by the mackinawite layer. Either way, the potential difference between the large surrounding steel surface covered by mackinawite (that was more positive) and the uncovered steel in the pits (that was more negative) was the driving force for a galvanic couple, which led to localized corrosion.

Based on the finding in the current study, there seems to be a threshold value of pH_2S which led to localized attack that was observed at concentrations up to 90 ppm H_2S in CO_2, but not at 150 ppm or more.[24] For the sake of the present argument, one can assume that this threshold was of the order of 100 ppm H_2S in CO_2 in the present study. It is expected that the threshold will vary with temperature and water chemistry (mostly affected by pH). At significantly higher temperatures and higher pH a lower threshold value is expected. It is of key importance to emphasize that this threshold actually refers to the ratio of H_2S to CO_2 gas partial pressures ($pH_2S/pCO_2 = 10^{-4}$) and not the actual H_2S gas concentration as reported from the field, which is different because of the presence of hydrocarbon gases.
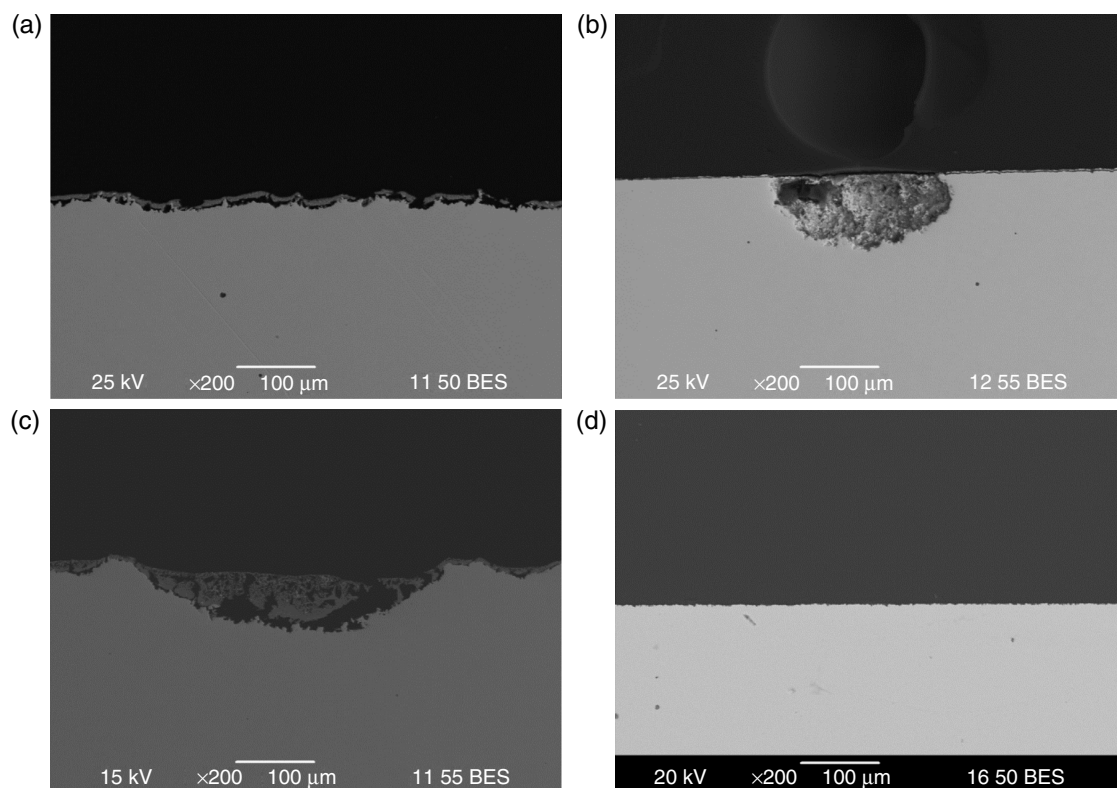
FIGURE 5. Cross-section image of X65 specimen after 6 d of exposure to an aqueous CO_2 solution at 30°C and pH 5.0: (a) no H_2S, (b) 40 ppm H_2S, (c) 90 ppm H_2S, and (d) 150 ppm H_2S, 1 wt% NaCl.
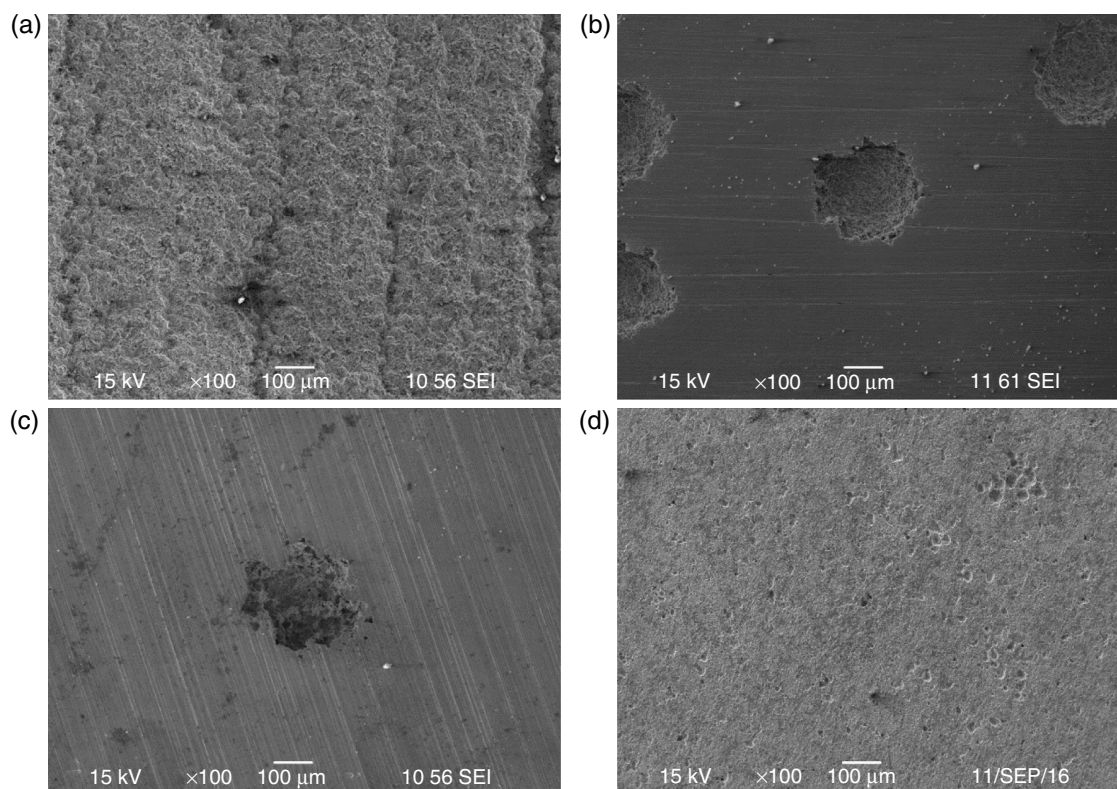

FIGURE 6. SEM image of X65 specimen after exposure to a saturated CO_2 solution at 30°C and pH 5.0 without corrosion product layer: (a) no H_2S, (b) 40 ppm H_2S, (c) 90 ppm H_2S, and (d) 150 ppm H_2S, 1 wt% NaCl, 6 d exposure.
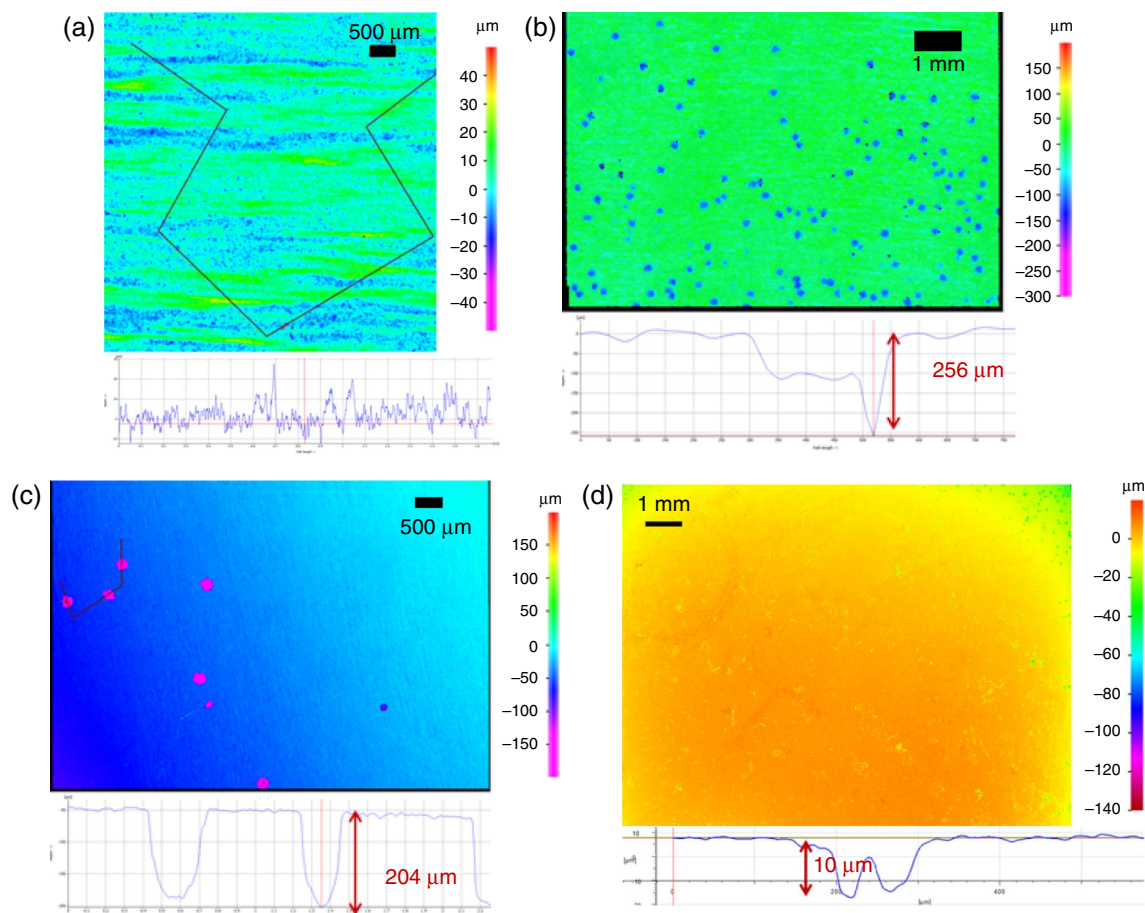
FIGURE 7. *Profilometry image of recovered X65 specimens after 6 d of exposure to an aqueous CO_2 solution at 30°C and pH 5.0 without corrosion product layer: (a) no H_2S, (b) 40 ppm H_2S, (c) 90 ppm H_2S, and (d) 150 ppm H_2S, 1 wt% NaCl.*
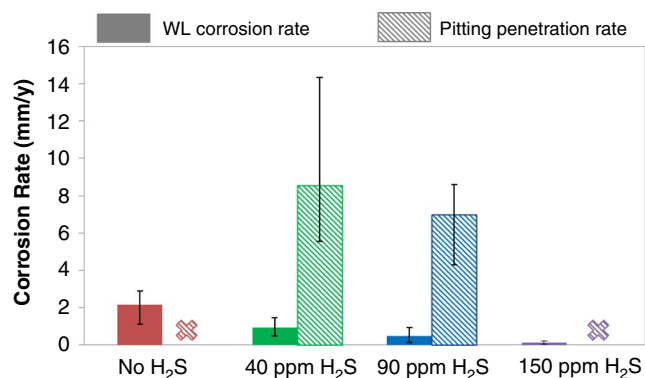

FIGURE 8. *Weight loss (WL) corrosion rate and pitting penetration rate of X65 specimen in aqueous CO_2 solution with and without H_2S at 30°C and pH 5.0, 1 wt% NaCl.*

CONCLUSIONS

In aqueous CO_2 environments with a trace amount of H_2S at low temperatures where the solution was undersaturated with respect to both iron carbonate and mackinawite:

❖ Mild steel underwent localized corrosion when there was not enough $[H_2S]_{aq}$ to form a stable mackinawite layer;

❖ Below 100 ppm H_2S (when the ratio of H_2S to CO_2 gas partial pressures was below 10^{-4}) localized attack was observed, while above this threshold the mackinawite layer provided a uniform protection to the steel surface;

❖ It is hypothesized that at lower H_2S concentrations, faults in the corrosion product layer allowed the corrosive species to reach the steel surface. This resulted in localized corrosion.

Engineering Research, Department of Chemical and Biomolecular Engineering at Ohio University enabling the use of the XRD equipment.

REFERENCES

1. J. Kvarekval, G. Svenningsen, "Effect of Iron Sulfide Deposits on Sour Corrosion of Carbon Steel," CORROSION 2016, paper no. 7313 (Houston, TX: NACE International, 2016).
2. W.R. Whitney, *Corrosion* 3 (1947): p. 331-340.
3. D.C. Bond, G.A. Marsh, *Corrosion* 6 (1950): p. 22-26.
4. F.H. Meyer, O.L. Riggs, R.L. McGlasson, J.D. Sudbury, *Corrosion* 14 (1957): p. 69-75.
5. P.H. Tewari, A.B. Campbell, *Can. J. Chem.* 57 (1979): p. 188-196.
6. D.E. Milliams, C.J. Kroese, "Aqueous Corrosion of Steel by H_2S and H_2S/CO_2 Mixture," in *Internal and External Protection of Pipes* (Cranfield, United Kingdom: British Hydromechanics Research Association, 1979), p. 205-214.
7. J.B. Sardisco, R.E. Pitts, *Corrosion* 21 (1965): p. 350-354.
8. J.B. Sardisco, R.E. Pitts, *Corrosion* 21 (1965): p. 245-253.
9. A. Dravnieks, C.H. Samans, *J. Electrochem. Soc.* 105 (1958): p. 183-191.
10. E.C. Greco, W.B. Wright, *Corrosion* 18 (1962): p. 119-124.
11. W.F. Rogers, J.A. Rowe, "Corrosion Effect of Hydrogen Sulfide and Carbon Dioxide in Oil Production," Fourth World Petroleum Congress (Rome, Italy: Carlo Colombo, 1955), p. 479-499.
12. S.N. Smith, M.W. Joosten, "Corrosion of Carbon Steel by H_2S in CO_2 Containing Oilfield Environments," CORROSION 2005, paper no. 06115 (Houston, TX: NACE, 2005).
13. P.W. Bolmer, *Corrosion* 21 (1965): p. 69-75.
14. B. Tribollet, J. Kittel, A. Meroufel, F. Ropital, F. Grosjean, E.M.M. Sutter, *Electrochim. Acta* 124 (2014): p. 46-51.
15. S.P. Ewing, *Corrosion* 11 (1955): p. 497-501.
16. J.B. Sardisco, W.B. Wright, E.C. Greco, *Corrosion* 19 (1963): p. 354-359.
17. X.B. Huang, Z.F. Yin, H.L. Li, Z.Q. Bai, W.Z. Zhao, *Corros. Eng. Sci. Technol.* 47 (2012): p. 78-83.
18. K. Videm, J. Kvarekvål, *Corros. Sci.* 51 (1995): p. 260-269.
19. Y.-S. Choi, S. Nešić, S. Ling, *Electrochim. Acta* 56 (2011): p. 1752-1760.
20. J. Kvarekval, R. Nyborg, M. Seiersten, "Corrosion Product Films on Carbon Steel in Semi-Sour CO_2/H_2S Environments," CORROSION 2002, paper no. 296 (Houston, TX: NACE, 2002).
21. J. Tang, Y. Shao, J. Guo, T. Zhang, G. Meng, F. Wang, *Corros. Sci.* 52 (2010): p. 2050-2058.
22. B. Brown, "H_2S Multiphase Flow Loop: CO_2 Corrosion in the Presence of Trace Amounts of Hydrogen Sulfide" (Master's thesis, Ohio University, 2004).
23. H. Fang, "Investigation of Localized Corrosion of Carbon Steel in H_2S Environments" (Ph.D. diss., Ohio University, 2012).
24. J. Ning, Y. Zheng, B. Brown, D. Young, S. Nešić, *Corrosion* 73 (2017): p. 155-168.
25. H. Fang, B. Brown, D. Young, S. Nešić, "Investigation of Elemental Sulfur Corrosion Mechanisms," CORROSION 2011, paper no. 398 (Houston, TX: NACE, 2011).
26. D.D. MacDonald, B. Robert, J.B. Hyne, *Corros. Sci.* 18 (1978): p. 411-425.
27. G. Schmitt, *Corrosion* 47 (1999): p. 285-308.
28. N. Yaakob, M. Singer, D. Young, "Elemental Sulfur Corrosion Behavior in the Presence of Sulfur Solvent and Monoethylene Glycol," CORROSION 2015, paper no. 5930 (Houston, TX: NACE, 2015).
29. D.F. Pridmore, R.T. Shuey, *Am. Mineral.* 61 (1976): p. 248-259.
30. C.I. Pearce, A.D. Pattrick, D.J. Vaughan, *Rev. Mineral. Geochem.* 61 (2006): p. 127-180.
31. R. Schieck, A. Hartmann, S. Fiechter, R. Konenkamp, H. Wetzel, *J. Mater. Res. Soc.* 5 (1990): p. 1567-1572.
32. P.K. Abraitis, R.A.D. Pattrick, D.J. Vaughan, *Int. J. Mine. Process* 74 (2004): p. 41-59.
33. D.J. Vaughan, J.R. Craig, *Mineral Chemistry of Metal Sulfides*, 1st ed. (New York, NY: Vail-Ballou, 1978), p. 86-103.
34. A.R. Lennie, K.E.R. England, D. Vaughan, *Am. Mineral.* 80 (1995): p. 960-967.
35. B.F.M. Pots, R.C. John, I.J. Rippon, M.J.J.S. Thomas, S.D. Kapusta, M.M. Girgis, T. Whitham, "Improvements on De Waard-Milliams Corrosion Prediction and Applications to Corrosion Management" CORROSION 2002, paper no. 235 (Houston, TX: NACE, 2002).
36. H. Fang, B. Brown, S. Nešić, *Corrosion* 67 (2011): p. 015001-1 to 015001-12.
37. N. Tsesmetzis, E.B. Alsop, A. Vigneron, F. Marcelis, I.M. Head, B.P. Lomans, "Microbial Community Analysis of Three Hydrocarbon Reservoir Cores Provides Valuable Insights for the Assessment of Reservoir Souring Potential," *Int. Biodeterior. Biodegrad.* in press (2017): doi: https://doi.org/10.1016/j.ibiod.2016.09.002.
38. K.J. Lee, "A Mechanistic Modeling of CO_2 Corrosion of Mild Steel in the Presence of H_2S" (Ph.D. diss., Ohio University, 2004).
39. N. Yaakob, F. Farelas, M. Singer, S. Nešić, D. Young, "Localized Top of the Line Corrosion in Marginally Sour Environments," CORROSION 2016, paper no. 7695 (Houston, TX: NACE, 2016).
40. N. Yaakob, "Top of the Line Corrosion in CO_2/H_2S Environments" (Ph.D. diss., Ohio University, 2015).
41. S. Navabzadeh Esmaeely, B. Bruce, S. Nešić, *Corrosion* 73 (2017): p. 144-154.
42. S. Al-Hassan, B. Mishra, D.L. Olson, M.M. Salama, *Corrosion* 54 (1998): p. 480-491.
43. F. Farelas, M. Galicia, B. Brown, S. Nešić, H. Castaneda, *Corros. Sci.* 52 (2010): p. 509-517.
44. A. Fragiel, R. Schouwenaarf, R. Guardian, R. Perez, *J. New Mater. Electrochem. Syst.* 8 (2005): p. 115-119.
45. D.N. Staicopolus, *J. Electrochem. Soc.* 110 (1963): p. 1121-1124.
46. W. Sun, S. Nešić, R.C. Woollam, *Corros. Sci.* 51 (2009): p. 1273-1276.
47. W. Sun, S. Nešić, R.C. Woollam, *Ind. Eng. Che. Res.* 1 (2008): p. 1738-1742.
48. O.M. Suleimenov, T.M. Seward, *Geochim. Cosmochim. Acta* 61 (1997): p. 5187-5198.
49. J. Han, B. Brown, D. Young, S. Nešić, *J. Appl. Electrochem.* 40 (2010): p. 683-690.
50. David Barthelmy, Mineralogy Database, http://webmineral.com/ (Sept. 02, 2016).
51. ASTM G1 (reapproved 2011), "Standard Practice for Preparing, Cleaning, and Evaluating Corrosion Test" (West Conshohocken, PA: ASTM, 2011).
52. B. Brown, "The Likelihood of Localized Corrosion in an H_2S/CO_2 Environment," CORROSION 2015, paper no. 5855 (Houston, TX: NACE, 2015).
53. K.J. Lee, S. Nešić, "The Effect of Trace Amount of H_2S on CO_2 Corrosion Investigated by Using the EIS Technique," CORROSION 2005, paper no. 630 (Houston, TX: NACE, 2005).
54. J. Lee, "A Mechanistic Modeling of CO_2 Corrosion of Mild Steel in the Presence of H_2S" (Ph.D. diss., Ohio University, 2004).
55. P. Sarin, V.L. Snoeyink, D.A. Lytle, W.M. Kriven, *J. Environ. Eng.* 130 (2004): p. 364-373.
56. W. Sun, S. Nešić, *Corrosion* 64 (2008): p. 334-346.
57. S. Nešić, "Carbon Dioxide Corrosion of Mild Steel," in *Uhlig's Corrosion Handbook*, ed. R. Winston Revie, 3rd ed. (Hoboken, NJ: John Wiley & Sons, Inc., 2011), p. 229-245.
58. K.J. Lee, S. Nešić, "EIS Investigation of CO_2/H_2S Corrosion," CORROSION 2004, paper no. 728 (Houston, TX: NACE, 2004).
59. D.A. Jones, *Principles and Prevention of Corrosion*, 2nd ed. (Upper Saddle River, NJ: Prentice-Hall, 1996), p. 168-198.